Journal of Naval Architecture and Marine Engineering
January, 2025
http://dx.doi.org/10.3329/jname.v22i1.70198 http://www.banglajol.info

NUMERICAL STUDY ON THE HYDRODYNAMIC PERFORMANCE OF A SELF-PROPELLED SUBMERSIBLE

M.A. Zenagui[1], S.E. Belhenniche[1], A. Miloud[1], O. Imine[2]
[1]Naval Aero-Hydrodynamic Laboratory, Marine Engineering Department, USTO MB, Oran 31000, Algeria.
[2]Aeronautics and Propulsion Systems Laboratory, Mechanical Engineering Department, USTO MB, Oran 31000 Algeria.

Abstract:

In this paper, a numerical study on the hydrodynamic performances of an autonomous unmanned vehicle (AUV) was carried out. For its propulsion, a model of a new seven-bladed propeller defined as stock propeller was made. Several numerical simulations were carried out, namely open water test, towing resistance test, and self-propulsion test. This study focuses on the thruster's ability to perform its task correctly for improved use. The examination of the propeller characteristics in open water test exhibits a better efficiency and the thrust can be improved by slightly adjusting the pitch distribution of the propeller. In the towing resistance test, wake behind the body was also investigated by studying axial velocity field in many transversal planes. Added to the self-propulsion test results, the evolution of the thrust magnitude in the wake by moving the thruster plane axially reveals that the required thrust level is reached far behind the actual position of the thruster disc. It is found that the ratio of thrusts with or without the presence of the body is equal neither to unity nor to the torque ratio.

Keywords: *Propeller, self-propulsion, RANS, numerical simulation, AUV.*

NOMENCLATURE

D	Propeller diameter
P/D	Pitch ratio
C	Chord length
T_{max}	Maximum blade section thickness
F_{max}	Maximum blade section camber
A_e/A_0	Expanded area ratio
J_A	Advance coefficient
Z	Blade number
t	Thrust deduction
C_D	Drag coefficient
n	Propeller rotational speed
L	Submarine length
C_p	Pressure coefficient
V_S	Submarine speed
w	Wake fraction
$\bar{P}$	Average pressure
K_T	Thrust coefficient
K_Q	Torque coefficient

Greek symbols

ρ	Density of water
S	Area plane
T	Propeller self-propulsion thrust
T_O	Propeller open water thrust
Q	Propeller self-propulsion torque
Q_O	Propeller open water torque
R_T	Total resistance
η_0	Propeller open water efficiency
η_B	Propeller behind a ship hull efficiency
η_H	Hull efficiency
η_D	Propulsif efficiency
η_R	Rotatif efficiency
μ	Dynamic viscosity
μ_T	Eddy viscosity
η_0	Propeller open water efficiency
η_B	Propeller behind a ship hull efficiency
η_H	Hull efficiency

1. Introduction

In many marine vehicles, the propeller is used as a means of propulsion. Geometry is considered well-defined in the propeller design when pitch, camber, thickness, chord, skew and rake distributions must be suitably determined in order to obtain the highest possible propulsive efficiency for thrust or delivered power requested.

The flow around the propeller has received increasing attention by Computational Fluid Dynamics (CFD). Previous studies showed the camber effect on the hydrodynamic efficiency of the propellers, pressure distribution, downstream velocity distribution, thrust and torque in open water conditions (Blevins (1984), Kerwin (1987) and Abdel-maksoud (1998)). By varying the number of propeller blades, it has been observed that the maximum hydrodynamic efficiency remains almost constant for propellers with three to seven blades and for practically the

 Received on Nov., 2023

same advance parameter. The main reason is that the effective angle of attack distributions, when the number of blades increases, does not change and the hydrodynamic efficiency is directly related to the camber distribution (Nouri et al. 2016, 2018).

Open water tests of the E1619 propeller were performed numerically using the CFD Ship-Iowa v4. The characteristics of the propeller were calculated, and the results were compared with experimental data as indicated in INSEAN (Di Felice et al. 2016). This study showed small effect of grid refinement on thrust and torque, but wake is affected.

Several investigations have highlighted the different methods for marine propeller analysis, such as; Large Eddy Simulation (LES) and Detached Eddy Simulation (DES) (Mizzi et al. 2016). According to previous studies, the RANS solver is influenced by the velocity field due to the propeller-hull interaction (Zhang et al. 2014). A comparative study for the propulsion process of a propeller was performed between the Scale Resolution Scale (SRS) and Reynolds Averaged Navier-Stokes (RANS) approaches. SRS models capture more turbulent structure detail than RANS method in transient flow capture (Cai et al. 2019). Optimization of a set of marine propellers is an option in marine propulsion research. A recent method has been proposed on the basis of the combination of RANS with a genetic algorithm coupled to the kriging algorithm in order to perform the optimization (Nouri et al. 2022)

Some efforts have been devoted to the development of computational methods to accurately predict hull resistance and power in recent years (Xhaferaj, 2022). Another technique is introduced by coupling two solvers for a flow simulation around the hull of a ship. The body force was calculated by means of PANMARE solver which is an in-house boundary element code and the flow field by ANSYS- CFX solver (Berger et al 2011). However, the unsteady boundary element method (BEM) for the propeller loading was used (Rijpkema et al. 2011). This approach allows reducing computational effort compared to a full RANS simulation. The obtained results have been compared with those of the RANS computations using fully resolved propeller geometry. The computations show good agreement with the experimental values.

Also, to optimize the ship design, three different ship hulls have been computed under self-propelled conditions using the CFD Ship-Iowa v4 (Carrica et al. 2014). The propeller is gridded as an overset object with a rotational velocity that is imposed by a speed controller to obtain the self-propulsion point. The results of the numerical self-propulsion tests were satisfactorily predicted since the comparison with the experimental data shows good agreement.

In this field, Lee et al. 2003, conducted simulations using ANSYS FLUENT 14.5 to improve the design of the submarine. The hydrodynamic performances of a 3000-ton class submarine built by Daewoo Shipbuilding and Marine Engineering Co. Ltd. have been evaluated and used. The resistance tests and self-propulsion tests with stock propeller have been conducted. The wake distribution measurements, streamline tests and flow field measurements have been carried out. In a recent study, Dogrul et al. [16] conducted numerical analyses for the Australian Joubert BB2 Submarine fitted with MARIN7371R propeller both in model scale and full scale. However, in the calculation, the propeller is modelled by a body force method. The scale effects on the resistance components and self-propulsion characteristics have been observed. Also, the ITTC 1978 performance prediction method was used for large-scale extrapolation and the results were compared with large-scale CFD results which showed good correlation.

Self-propulsion simulations of the DARPA (Defence Advanced Research Projects Agency) submarine with appendages and the E1619 propeller were carried out in a model scale and the resulting propeller performance was analysed (Chase et al. 2013). The Model E1619 propeller has been used with several DARPA submarine configurations in numerous studies devoted to numerical self-propulsion tests (Dogrul et al. (2017), Sezen et al. (2018) and Chase et al. (2013)). Two techniques have been employed for self-propulsion simulations: the body force method and the model propeller itself mounted behind the submarine hull.

Carrica et al. (2019) conducted a numerical investigation of Joubert BB2 submarine self-propelled near the free surface in calm water and waves. The dynamic overset mesh was adopted using different grids by a factor of $\sqrt{2}$ for each coarsening step. The authors reveal that propeller revolution and thrust increase as the submarine gets closer to the free surface. They also revealed that thrust and torque coefficients are a little bit lower in waves than in calm water due to the higher values of inflow velocities into the propeller disc.

Donglei Zhang et al. (2022) carried out an interaction study between KVLCC2 ship and DARPA Suboff submarine. Three different grids were used: coarse, medium, and fine for numerical uncertainty study. The obtained results show that the vertical distance between DARPA Suboff submarine and KVLCC2 has an influence on submarine. The authors revealed that as the forward speed of submarine and tanker increases, the vertical force and pitching moment will be higher. A numerical investigation of a submarine sailing near a free surface was performed by Kai Dong et al. (2022). Three different submerged depths ranging from 1.1D to 3.3D were selected for calm water and irregular waves conditions. The obtained results for calm water show that as the submarine is sailing near the free surface, the resistance, lift and bow-app moment increase when the depth decrease. However, they decrease with greater submerged depths. For the irregular waves, the results show considerable fluctuations of hydrodynamic forces and moments at deeper submerged depths.

The present paper deals with a study of an autonomous unmanned vehicle (AUV) self-propulsion test by numerical simulation. The stock propeller used for this test is created for this purpose from a basic model of highly skewed propellers usually used in submarines and its geometry is defined in the present work. It is essential to carry out a numerical test in open water in order to determine the propeller characteristics. The body chosen for the AUV is a bare hull of a DREA (Defence Research Establishment Atlantic) standard submarine. All the geometric details are given in this study. The resistance test of this marine vehicle is necessary to determine the suction and wake coefficient, respectively, in the propeller disk. Particular attention is paid to the wake of the AUV, and emphasis is placed on the axial velocity in the flow field behind the AUV. Thus, in this study, calculations are performed to determine the axial velocity field in many transverse planes, and then the average wake coefficient at each plane is calculated. The purpose of this investigation is to verify the validity of the two methods, "thrust identity" and "torque identity", when carrying out the self-propulsion test.

The numerical simulations carried out are respectively tests in open water, towing resistance and self-propulsion. All tests were performed using the ANSYS Fluent 14.5 solver. The flow was considered totally turbulent, incompressible, and steady. The "k-ε " turbulence model was applied for all numerical tests.

2. Geometry of the Propelled Submersible

2.1 Propeller geometry

The propeller, used in this study, is characterized mainly by high values of skew distribution, as shown in Figure 1 and 2. The particulars of propeller geometry are also given through the respective radial distributions of the chord, pitch, camber, thickness and skew as illustrated in table 1 and 2.

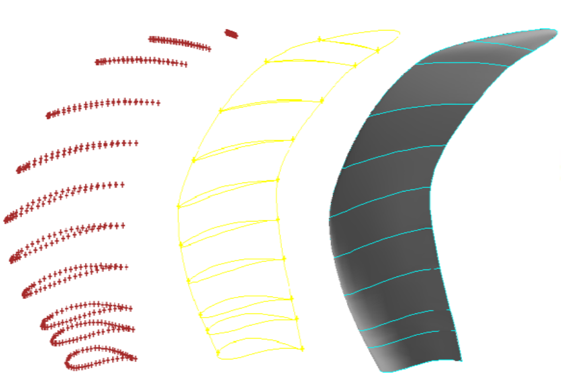

Fig. 1: Propeller drawing steps

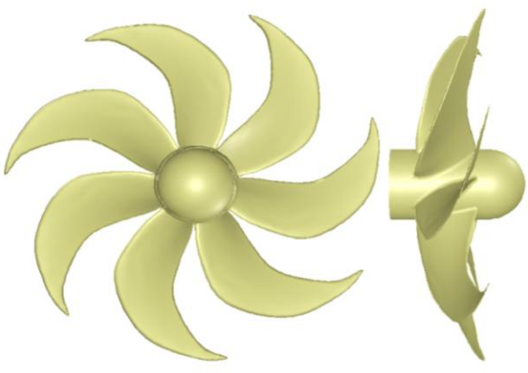

Fig. 2: 3-D view of model propeller developed.

Table 1: Radial distributions of the geometric characteristics of the tested propeller

r/R [-]	*C* [m]	F_{max}/C [-]	T_{max}/c [-]	*P/D* [-]	*Skew* [m]
0.18	0.18692	0.02845	0.04585	1.16292	-1.96824

0.25	0.18996	0.02964	0.04071	1.16881	-2.91066
0.3	0.19347	0.02948	0.03712	1.17946	-3.26094
0.4	0.18806	0.02677	0.03047	1.18877	-3.22758
0.5	0.18692	0.02201	0.02459	1.16881	-2.31852
0.6	0.18996	0.01732	0.01947	1.16292	-0.6255
0.7	0.18622	0.01404	0.01492	1.15000	3.42774
0.8	0.17111	0.012	0.01073	1.10374	8.14032
0.9	0.13741	0.01044	0.00693	1.03912	13.07862
0.95	0.0921	0.01007	0.00528	1.00185	17.00542
1	0.0163	0.0087	0.00369	0.96124	21.50612

Therefore, spatial point coordinates of each section are exported to the pre-processor Gambit describing a shape of propeller blade. Appropriate points are connected through curves by using the spline function to create faces and blade volume, as shown in Figure 1. The shaft is also connected to the propeller root blades by using T-junction sequence on Gambit.

Table 2: Main particulars of the tested propeller model

N°	Characteristics	Open Water	Self-Propulsion
1	D [mm]	485	262
2	P/D [-]	1.15	1.15
3	Z [-]	7	7
4	A_E/A_0 [-]	0.608	0.608
5	Rotation	Clockwise	Clockwise

2.2 Submersible body

The DREA submarine geometry has been obtained from the Riegels profile, type D2, having an axisymmetric hull form with an optimal ratio, where L is the hull length and d is the maximum diameter of the hull. Riegels (1961) specified the profile radius in three regions nose, mid body (circular cylinder) and tail. For the appendages, both rudders and stern planes have NACA four digit airfoil thickness profiles (Abbott et al., 1959). The DREA geometry is shown in Figure 3.

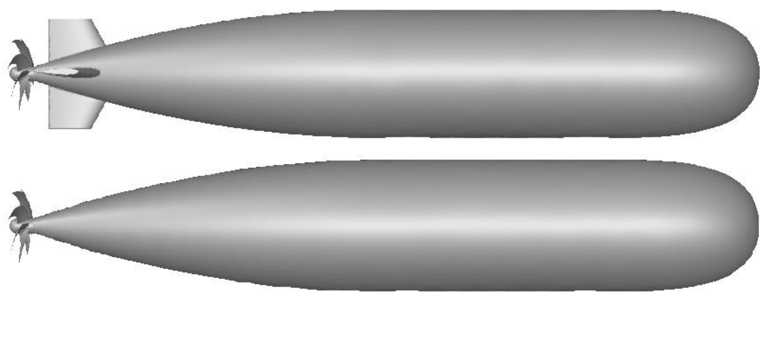

Fig. 3 DREA submarine geometry

3. Governing Equations

3.1 Navier-stokes equations

The governing equations adapted in this study for propeller and underwater vehicle simulations are the incompressible Navier Stokes equations for the steady turbulent flow. In terms of constant density flows, the continuity and momentum equations of RANS can be expressed by the following equations:

$$\frac{\partial u_i}{\partial x_i} = 0 \tag{1}$$

$$\rho \frac{\partial \overline{u_i}}{\partial t} + \rho \frac{\partial \overline{u_i u_j}}{\partial x_j} = -\frac{\partial \overline{P}}{\partial x_j} + \mu \frac{\partial^2 \overline{u_i}}{\partial x_j^2} - \rho \frac{\partial}{\partial x_j} \overline{u'_j u'_i} \tag{2}$$

Boussinesq (1877) proposed the relation between the Reynolds stresses and the mean velocity gradients, which is commonly known as Boussinesq hypothesis (Kalkan et al. 2014) and given as:

$$-\rho u'_j u'_i = -\mu_t \left(\frac{\partial \overline{u_j}}{\partial x_i} + \frac{\partial \overline{u_i}}{\partial x_j} \right) + \frac{2}{3} \delta_{ij} \rho k \tag{3}$$

Where δ_{ij} represents the Kronecker delta function,

$$\delta_{ij} = \begin{cases} 1 \text{if } i = j \\ 0 \text{if } i \neq j \end{cases}$$

By introducing equation (3) in equation (2), the fluctuating quantities will be replaced by the Eddy viscosity μ_t .

Cable (2009) has rewritten the RANS equation again as follows:

$$\rho \frac{\partial \overline{u_i}}{\partial t} + \rho \frac{\partial \overline{u_i u_j}}{\partial x_j} = -\frac{\partial \overline{P}}{\partial x_j} + (\mu + \mu_t) \frac{\partial^2 \overline{u_i}}{\partial x_j^2} \tag{4}$$

Applying the Boussinesq hypothesis to the RANS equation, it is quite easy to close the equation system by modelling the turbulent viscosity. Although the first efforts trace to 1945, the commonly accepted representation of "k-ε" turbulence model has been developed by Launder et al. (1974)

3.2 Computational domain grid and boundary conditions:

In order to study the propeller performances in open water (uniform flow), a periodic cylindrical control volume in Figure 4 has been considered around the propeller with velocity inlet, pressure outlet and periodic boundary conditions. The domain distances have been considered sufficiently large to prevent blockage effects on the propeller hydrodynamic performance characteristics. The computational domain is defined at 1.5D for inflow, 3.5D for outflow and 1.4D for Open water or (Slip wall), where D is propeller diameter Belhenniche et al. (2012).

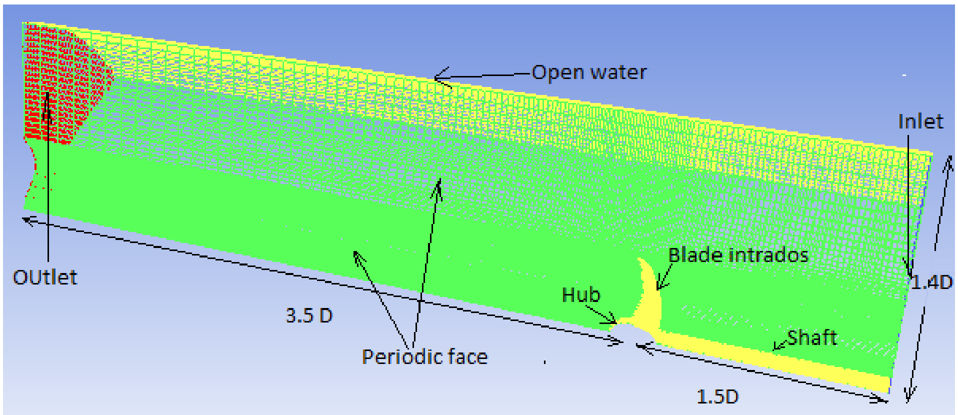

Fig. 4: Periodic boundary condition and domain length

An unstructured hybrid mesh has been applied for grid generation. A fine tetrahedral mesh has been used in blade and hub zone as shown in Figure 5. A Hexahedral mesh has been used for inflow, outflow and up flow regions. The grid aspect ratio is gradually increased to decrease solution costs. More than one million elements have been created for the whole domain grid, as demonstrated in Figure 4.

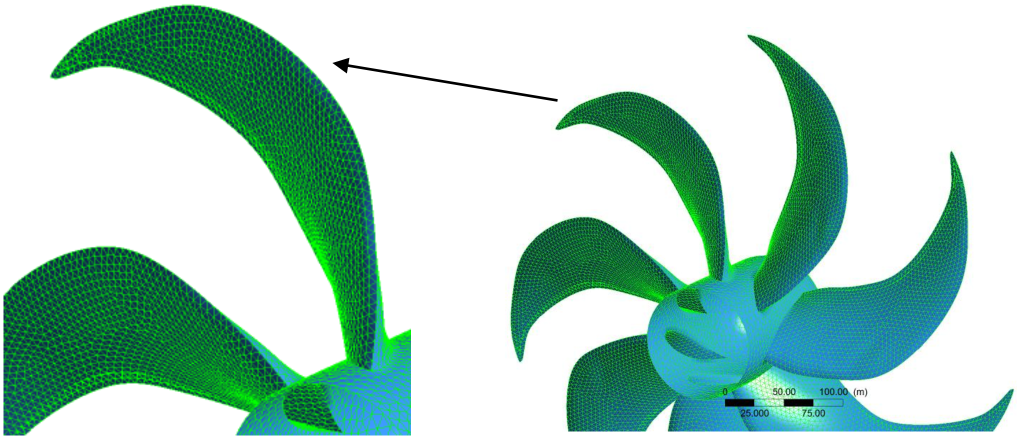

Fig. 5: Tetrahedral mesh in blade and hub zone

However, for resistance and self-propulsion analysis, a parallelepipedic domain has been used in order to simulate a flow around the submarine hull without or fitted with the tested propeller. The inlet face is located at 0.7L from the hull, in the right side. The outlet face is at 2.3L behind the hull in the left side, and the lateral faces at 2.5L and 5L from the hull are considered as virtual wall. The submarine hull is defined as no-slip wall, as mentioned in Figure 6 and 7, where L is the submarine length.

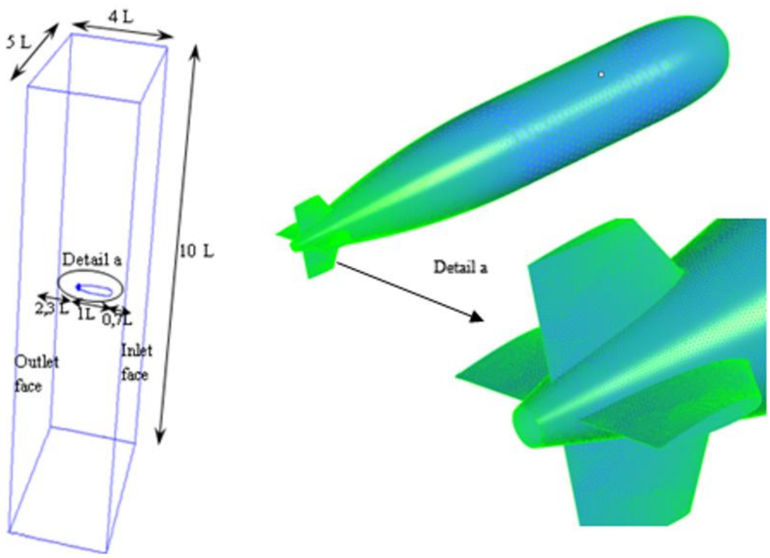

Fig. 6: Computational domain lengths, surface mesh and boundary conditions of the appended hull

The computational domain has been meshed by unstructured tetrahedral elements. The mesh has also been refined in the bow and the stern of the hull. The unstructured mesh of the hull is given in Figure 6, detail “a”. For self-propulsion analysis, two computational domains have been used. The first domain computes a linear flow around the submarine hull. The second is the cylindrical domain behind the submarine hull and simulates the flow around the propeller by incoming velocity behind the hull. By using a frame motion, the rotational speed of the tested propeller has been adjusted. Both domains are connected by cylinder and base mesh interfaces in order to model the interaction of the hull and the propeller more accurately. A tetrahedral mesh structure has been employed, and a fine mesh has been created around the propeller and the wake zone behind the propelled submarine. The domain lengths, the boundary conditions, and the mesh generated for the self-propulsion are shown in Figure 7, detail “b”.

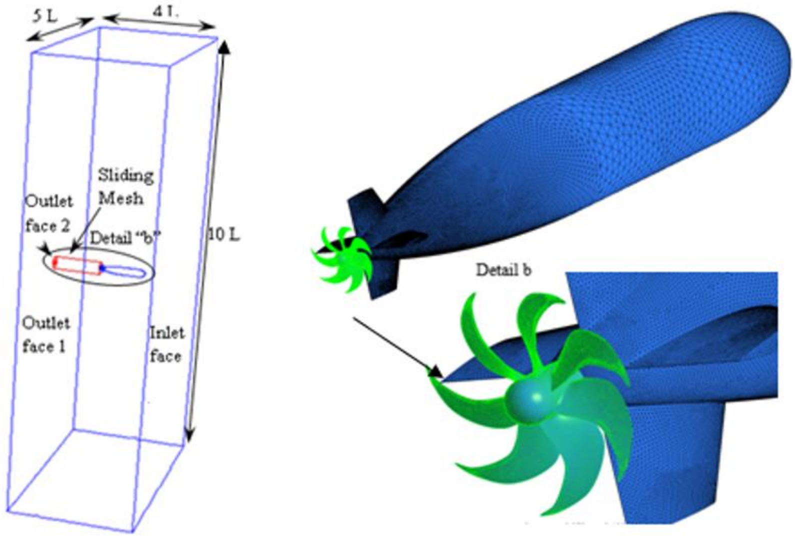

Fig. 7: Computational domain lengths, surface mesh and boundary conditions of the submarine fitted with the tested propeller.

For the momentum equations and all runs, a second-order upwind scheme has been used for convection, and a second-order scheme has been used for diffusion. The SIMPLE scheme has been adjusted for the pressure-velocity coupling. Finally, the first-order upwind scheme has been used for the turbulence equations.

4. Simulation Results and Discussion

Three types of numerical simulations have been performed in this study to determine hydrodynamic performances of bare hull submersible with appendages, isolated propeller and propelled submersible. These are the tests of resistance, open water, and self-propulsion.

Before starting the calculations for each case, it is necessary to carry out a study of the solution sensitivity. The recommendations stipulate that the grid study should use a minimum of three meshes on the domain calculation; fine, medium, and coarse grids (25th ITTC Resistance Committee, 2008). A grid refinemen0t ratio of $\sqrt{2}$ was adopted between medium-fine grid lengths and coarse-medium ones (Stern et al. 1999) This choice is crucial in sensitivity studies especially for unstructured mesh system (ITTC – Recommended Procedures and Guidelines, 2011).

4.1 Isolated propeller analysis

4.1.1 Study of solution sensitivity

The study of grid independency has been carried out for $J_A = 0.894$ by considering four grids whose node values are shown in Table 3. It is noticed that the resulting K_T has been compared with the one of E1619. In appearance, this last propeller resembles the tested propeller. Their skew and chord distributions respectively are almost similar. Thus, the experimental thrust coefficient of the E1619 model propeller is $K_T = 0.1638$.

For more verification of the grid sensitivity, it is important to note that the refinement ratio must remain approximately the same between coarse and medium mesh, medium and fine mesh and fine and very fine mesh. The refinement ratio is expressed as Degiuli e al. (2021):

$$r_{43} = \sqrt[3]{\frac{N_3}{N_4}};\ r_{32} = \sqrt[3]{\frac{N_2}{N_3}};\ r_{21} = \sqrt[3]{\frac{N_1}{N_2}} \tag{5}$$

Where N is the number of cells of each mesh, index 1 represents the very fine mesh, index 2 represents the fine mesh, index 3 represents the medium mesh and index 4 represents the coarse mesh. Different grid sizes and the corresponding refinement ratios are given in Table 3. The results in Table 4 show that the gap of K_T between the two propellers increases with the increase of the node number. Therefore, the refinement of the mesh improves the result as it is expected. Considering the two aspects, best efficiency in the prediction of thrust coefficient and low computational times, the second configuration has been chosen for the following calculation.

Table 3: Cells number and their refinement ratios

Model	N_4	N_3	N_2	N_1	r_{43}	r_{32}	r_{21}
Tested propeller	*671762*	945864	1304656	1876255	1.12	1.11	1.12

Table 4: Comparison of the numerical and experimental E1619 results

N°	Grid type	Nodes number	$K_{T\,\mathrm{Num}}$	Relative error %
1	Very fine	733362	0.1536	6.64
2	Fine	518345	0.1533	6.84
3	Medium	366660	0.1532	6.92
4	Coarse	258981	0.1529	7.12

4.1.2 Open water test

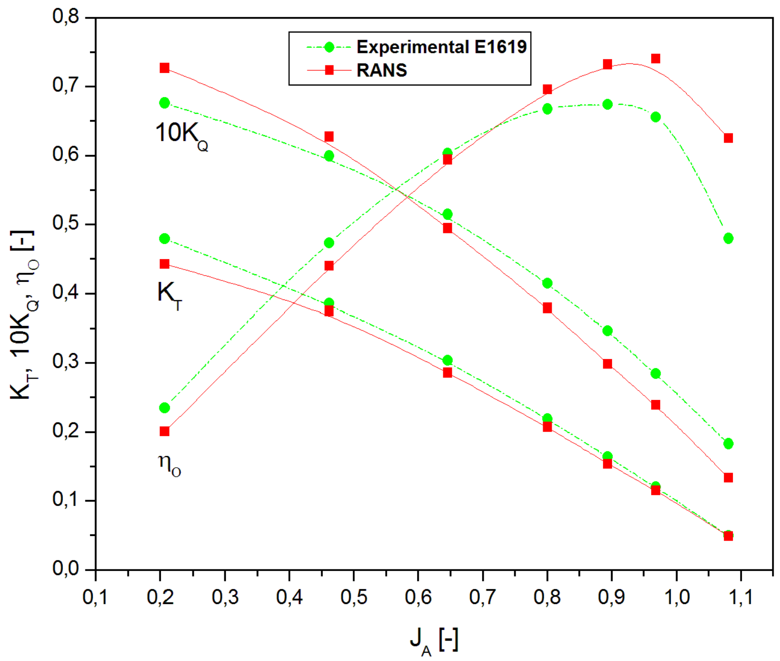

Fig. 8: Comparison of thrust torque coefficients and efficiency of modified propeller with E1619 propeller

Propeller investigation in open water has been performed by maintaining rotation speed constant with a value of $n = 368\ rpm$. The obtained results of the tested propeller model have been compared with the experimental data of the E1619 propeller model tested in INSEAN (Rijpkema et al., 2013, Carrica et al., 2010). In Fig. 8, the curves of performances are presented for the two propellers. It can be seen that the difference in KT K_T between the compared propellers is smaller than for in K_Q.This finding is also confirmed by all similar studies (Dogrul, 2022, Di Felice et al., 2009 and Xhaferaj, 2022). A good agreement is observed for the overall interval of J_A.

Figures 9 and 10 show the contours of the pressure coefficient on the faces of the tested propeller where the suction area (negative Cp values) is dominant on the back face. On the front face, although the pressure section is large, negative Cp pressure values also exist on small area near the hub from the leading edge. This means that the pitch angle must be adjusted slightly in this zone to eliminate the low pressure and increase thrust on this propeller.

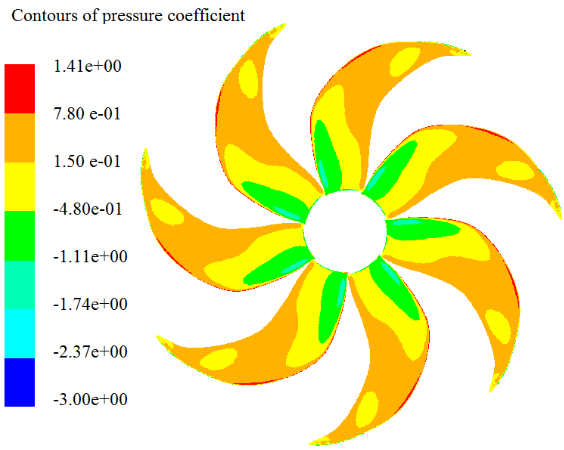

Fig. 9: Pressure coefficient around the front face of the propeller at $J_A = 0.89$

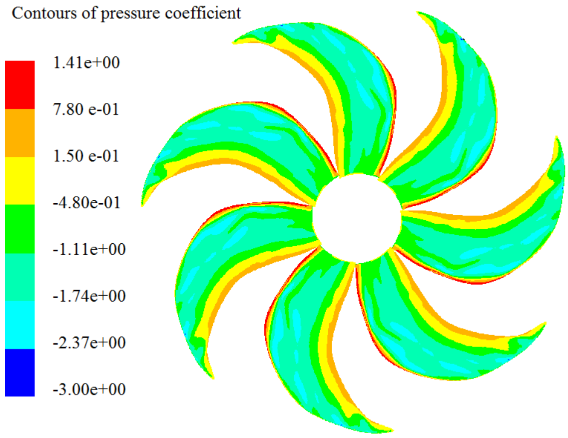

Fig. 10: Pressure coefficient around the back face of propeller at $J_A = 0.89$

4.2 Resistance Analysis

4.2.1 Study of solution sensitivity

For the grid independency study, calculations have been performed on the appended hull of the model submarine (DREA Suboff) without a propeller to determine the drag coefficient. The simulations have been done in water as fluids using a model with a length of $L = 2.7m$ in a flow that has a speed of $V_s = 8.56\, m/s$. All numerical results have been compared with the experimental data tested and reported by Baker (2004).

Table 5: Comparison of the numerical results and experimental data for the bare hull DREA submarine

N°	Grid Type	Nodes Number	CD_{Exp} (Baker, 2004).	CD_{Num}
1	Very fine	570185	0,00123	0.00146
2	Fine	403678	$\pm \Delta C_D = 6.3 \times 10^{-4}$	0.00154
3	Medium	286182	$\begin{cases} C_{D\,Exp\_max} = 0.00155 \\ C_{D\,Exp\_min} = 0.00092 \end{cases}$	0.00155
4	Coarse	202516		0.00175

Table 4 compares the drag coefficient for different meshes and shows the error margin between the experimental C_D and the calculated one. The error decreases with an increase in nodes number. Therefore, a compromise between acceptable time simulation and the accurate solution is adopted by choosing the fine grid for the following computations.

4.2.2 Towing resistance test

The precedent CFD simulation is continued by varying the value of water speed to obtain the resistance curve relative to the submarine's model. Figure 11 shows the resistance curve of the appended submarine as a result deriving from the last numerical test. As it can be seen, the trend of this physical quantity is typically increasing as the square of the flow speed. This suggests that the drag coefficient remains constant in the explored speed interval.

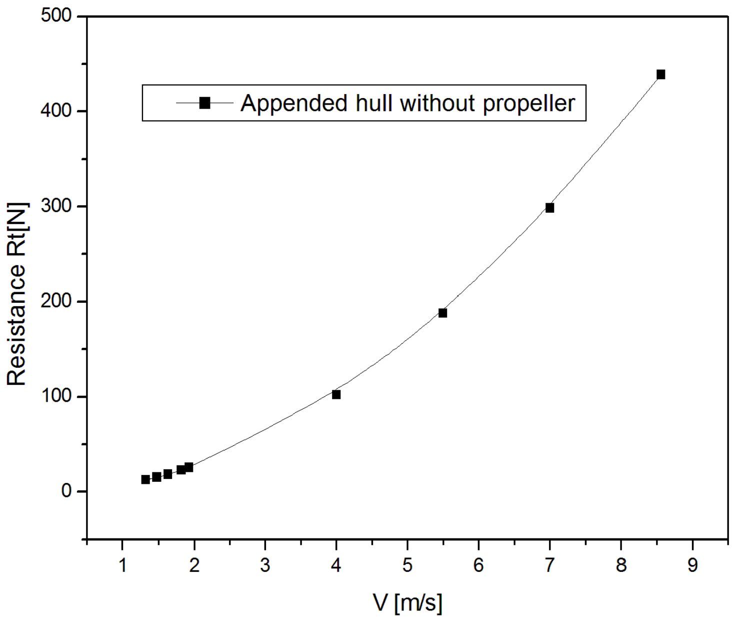

Fig. 11: Towing resistance of the appended DREA submarine

Figures 12 and 13 illustrate the contours of the pressure coefficient on the DREA sub-off body obtained by the numerical test for a value of the upstream velocity $V_s = 1.82\ {}^{m}/_{s}$. Mainly, it is noticed that a low-pressure zone with a negative value of Cp is localized near the nose. It is due to the acceleration of the flow when fluid particles go up the body from the nose. This acceleration also occurs moderately when fluid particles go down the body at the start of its conical shape or go over the appendage surfaces near their leading edges. On the other hand, the pressure remains quasi-constant for the length of the central part of the body.

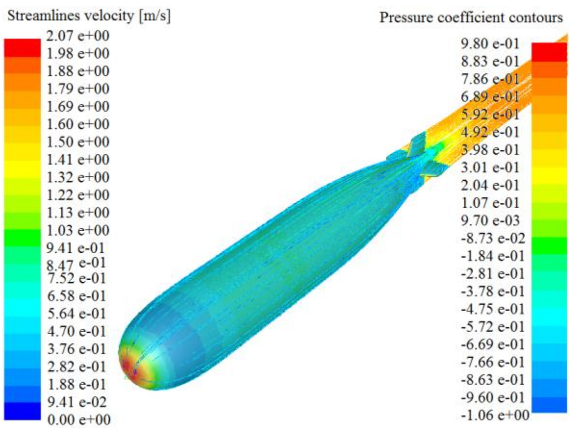

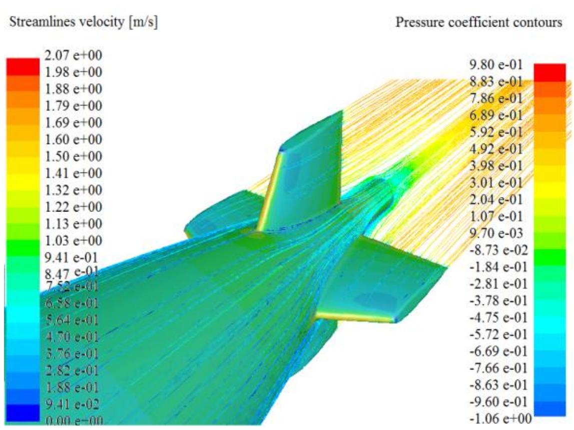

Fig. 12: Wall pressure distribution and pathlines around DREA hull at $V_s = 1.82\ {}^{m}/_{s}$

Fig. 13: Pressure coefficient around the back face of propeller at $V_s = 1.82\ {}^{m}/_{s}$

Figure 14 represents the mean axial velocity in the wake of the submersible without the propeller for the upstream velocity value of $V_s = 1.82\ m/s$. Three planes have been chosen from the position of the propulsor disc, $X/D = 0,\ 0.38\ and\ 0.76$. The exam of these charts reveals that there is no symmetry of revolution for the axial velocity distribution. This is very clear that the appendages with its four wings as well as for the hub have a visible trace. The lack of the mean axial velocity in the wake, as it can be observed mainly in the central part, disappears progressively away from the plane. Then, the wake fraction in the propulsor plane is calculated for each tested velocity rotation, as shown in Table 6 with an average value of $w = 0.289$.

Where:

$$w = \frac{1}{S}\int\left(1 - \frac{V_A}{V_S}\right)\ ds \qquad (6)$$

V_A : Local axial velocity

S : Area plane

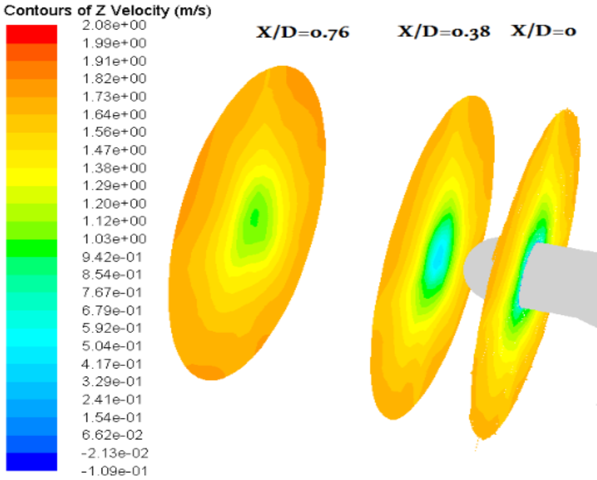

Fig. 14: Axial velocity distributions at $X/D = 0, 0.38\ and\ 0.76$ of DREA submarine for $V_s = 1.82\ m/s$

Table 6: Nominal wake coefficient for each average velocity at propeller plane

$V_S\ (m/s)$	1.3332	1.4827	1.6323	1.8218	1.9315	4	5.5	7	8.56
$V_A\ (m/s)$	0.9253	1.0291	1.137	1.2732	1.3544	2.8808	4.0026	5.1328	6.3124
w	0.306	0.306	0.303	0.301	0.299	0.280	0.272	0.267	0.263

4.3 Self-propulsion analysis

In this test, the flow around the propelled body model has been numerically simulated by varying the upstream velocity. During this test, convergence is reached by following a technique (friction deduction force) that consists of a value of the upstream velocity to look for, intuitively, the rotation speed of the propeller that guarantees the balance between propeller thrust and body drag. The calculations, performed in a steady state, require more time since this approach is not automated. Indeed, to find the point of self-propulsion, the difference between thrust and resistance during the calculation is checked. To achieve the equilibrium of forces, the magnitude of the angular velocity is gradually modified. This is done until the difference becomes zero. Kinaci et al. (2020) discussed the method to find the self-propulsion point. The grid mesh, inspired by the precedent studies of sensitivity solutions, has a node number of 769923.

The most important result of the self-propulsion test is resumed by the curve giving the variation of the upstream velocity against the rotation speed at the balance point. Figure 15 shows linear trend of the curve due to the fact that propeller has to work for a unique advance ratio which corresponds to the optimal conditions. In this test, the advance coefficient, calculated at the propeller disc, is determined from the slope of the curve and is found to be $J_A = 0.81$. By localizing these values on the efficiency curve of the open water characteristics, these points are not corresponding to the maximum efficiency but are slightly shifted.

Figure 16 illustrates the respective variations of thrust, torque and power against upstream velocity. The power curve follows a cubic trend as a consequence of the linear relationship between n and V, while thrust and torque follow parabolic trends.

In the Figure 17, the curve of the resistance is also plotted obviously with a magnitude lower to the one of the thrust. In this context, the thrust deduction has been calculated for each tested rotation velocity, and the values are shown in Table 7.

Table 7: Thrust deduction factor for each rotational speed

$n(rpm)$	270	300	330	368	390	802.5	1101	1398.5	1708
$V_s\left({}^{m}\!/_{s}\right)$	1.3332	1.4827	1.6323	1.8218	1.9315	4	5.5	7	8.56
$T(N)$	14.125	17.285	20.756	25.572	28.588	114.1	209.6	332.2	488.13
$R_T(N)$	12.631	15.467	18.571	22.881	25.571	102.39	188.19	298.43	438.72
t	0.106	0.105	0.105	0.105	0.106	0.103	0.102	0.102	0.101

$$t = 1 - \frac{R_T}{T} \tag{7}$$

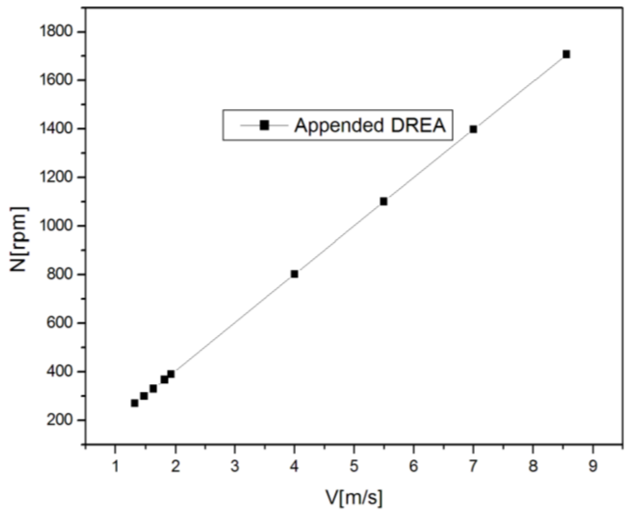

Fig. 15: Variation of the rotational speed against the upstream velocity at the balance point

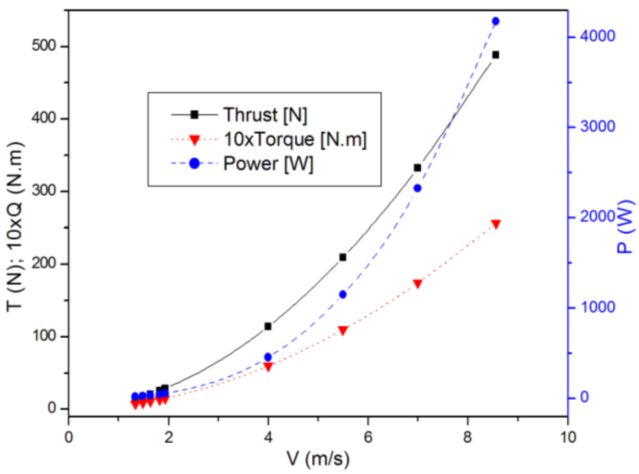

Fig. 16: Propeller characteristics Thrust (T), Torque (Q) and Power (P) against upstream velocity

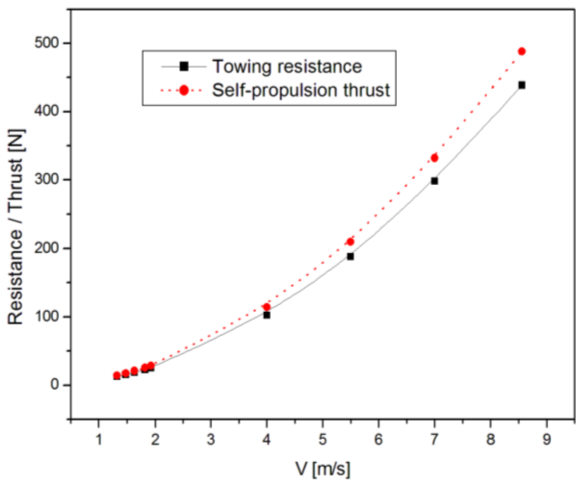

Fig. 17: Variation of the developed thrust by the propeller and towing resistance against the upstream velocity

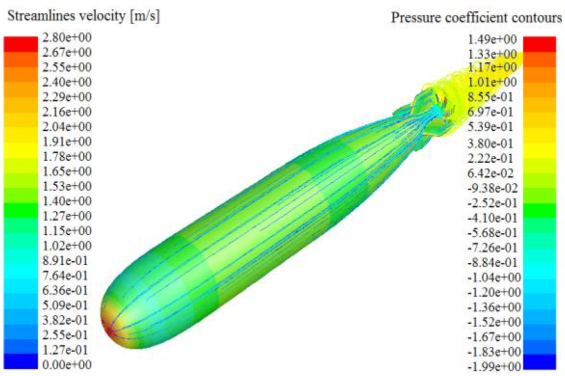

Fig. 18: Wall pressure distribution and pathlines around propelled DREA hull at $V_s = 1.82\, {}^{m}\!/\!_{s}$

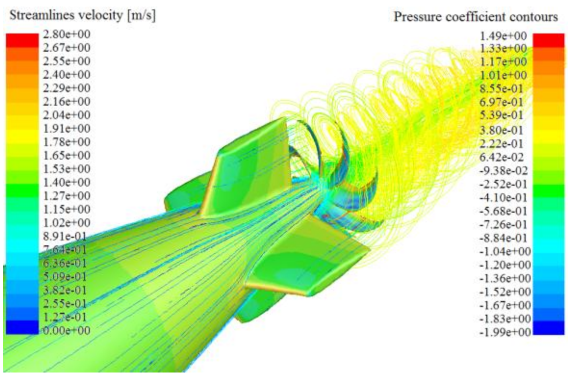

Fig. 19: Zoomed wall Pressure coefficient and pathlines at $V_s = 1.82\, {}^{m}\!/\!_{s}$

The measure of the mean axial velocity in the propulsor plane behind the submersible, without the propeller, allows drawing the axial wake field which is used in the design of the propeller. Indeed, the deduced wake fraction is applied to determine the advance coefficient and calculate the thrust from the open water characteristics. It is interesting to study the evolution of the thrust magnitude in the wake by moving the propulsor plane hypothetically in the X axis. Figures 20 and 21 illustrate this behavior for different values of rotational velocity. It is noticed that thrust decreases along this axis. The required thrust level is reached away behind the real position of the propulsor disc. The obtained curves seem to be parallel, denoting a same reduction of the thrust. It has been deduced from these remarks that the coefficient thrust ratio T_0/T is different to unity (Bertram (2000), Carlton (2019) and Molland (2017)), as shown in Table 8.

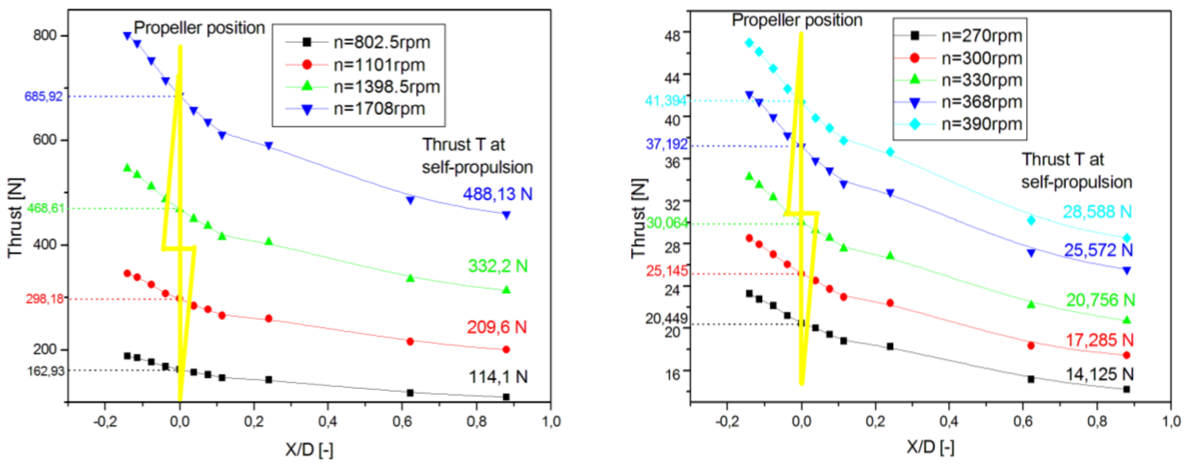

Fig. 20 Thrust in DREA wake for rotational speeds tested.

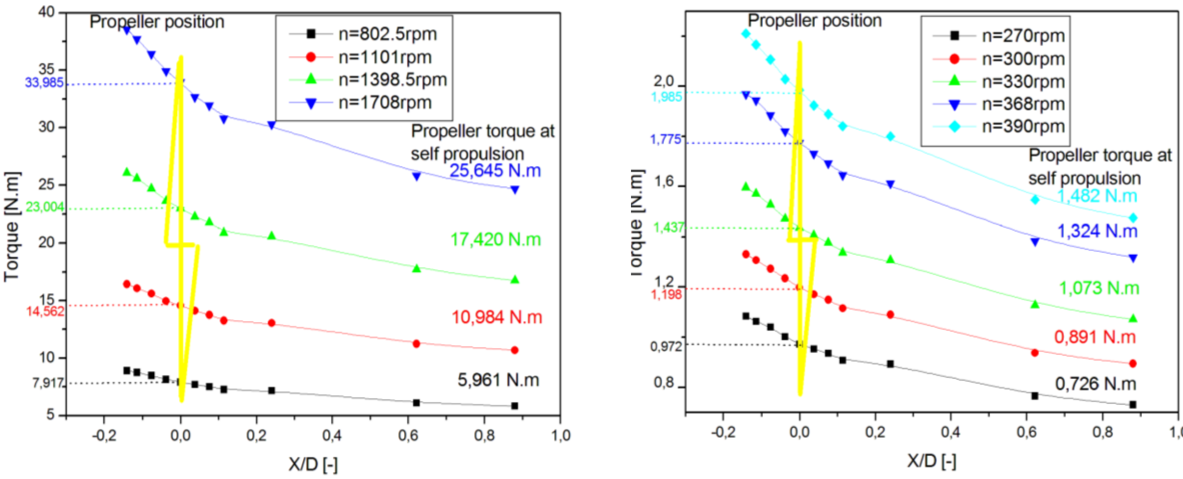

Fig. 21 Propeller torque in DREA wake for rotational speeds tested.

In the interval of the tested rotation velocity, this ratio remains roughly constant as well as for the ratio Q_0/Q, as shown in Table 8. The average values are respectively $T_0/T = 1{,}435$, $Q_0/Q = 1{,}333$. The propulsive efficiency is also calculated and seems to be almost constant for a wide range of propeller revolution. Its value ($\eta_D = 0{,}817$) is higher and this is probably due to the flow behind the body which is slightly disturbed compared to ship hull wake.

Table 8 Thrust and torque ratios for each rotational speed

Rotational speed (*rpm*)	270	300	330	368	390	802.5	1101	1398.5	1708
Thrust (N) self-propulsion T	14.125	17.285	20.765	25.588	28.588	114.1	209.6	332.2	488.13

Thrust (N) open water T_0	20.449	25.145	30.064	37.192	41.394	162.9	298.2	468.61	685.92
Torque ($N.m$) self-propulsion Q	0.726	0.891	1.073	1.324	1.482	5.961	10.98	17.42	25.645
Torque ($N.m$) open water Q_0	0.972	1.198	1.437	1.77	1.98	7.917	14.56	23.004	33.985
T_0/T	1.448	1.455	1.448	1.454	1.448	1.428	1.423	1.411	1.405
Q_0/Q	1.338	1.344	1.339	1.336	1.336	1.328	1.326	1.321	1.325
$\eta_R = Q_0.T/Q.T_0$	0.924	0.924	0.925	0.923	0.919	0.930	0.932	0.936	0.943
t	0.106	0.105	0.105	0.105	0.106	0.103	0.102	0.102	0.101
w	0.306	0.306	0.303	0.301	0.299	0.280	0.272	0.267	0.263
$V_A\left(m/s\right)$	0.9253	1.0291	1.137	1.2732	1.3544	2.8808	4.0026	5.1328	6.3124
$\eta_H = \frac{1-t}{1-w}$	1.288	1.290	1.284	1.280	1.275	1.246	1.234	1.225	1.220
$\eta_O = \frac{30T_0.V_A}{\pi n Q_0}$	0,688	0.688	0.688	0.694	0.693	0.705	0.711	0.714	0.712
$\eta_D = \eta_O\ \eta_R\ \eta_H$	0,819	0.820	0.817	0.820	0.812	0.817	0.818	0.817	0.819

5. Conclusion

A comprehensive study has been done using the CFD method in order to predict the self-propulsion performance of the DREA Suboff form. The numerical analysis has been done using the optimum grid number determined by verification and validation processes.

- Open water analysis has been carried out for the designed submarine propeller in the present study. The results of the test show that the created propeller exhibits a slightly lower value of thrust coefficient than the one of the E1619 propeller. The exam of pressure contours reveals an existence of a low-pressure zone on the propeller face which can be eliminated by adjusting slightly pitch distribution in order to increase thrust. While, the torque coefficient of the designed propeller is significantly higher compared to that of the E1619. This has a positive impact on the designed propeller performances.

- Total resistance distribution of the submarine's appended model has been also computationally determined. The comparison of the present result with the experimental data is satisfactory. Different sections of axial velocity contours in the wake of the DREA Suboff model have been taken front and back of the propeller disc in order to determine the evolution of the wake fraction.

- Self-propulsion performance analysis shows that the advance coefficient of the propeller remains constant and corresponds to nearly maximal efficiency of the open water test. The results reveal also that, at the presumed propeller disc position and for different tested rotation velocities, the thrust and torque produced by the propeller are very different to the ones given by the open water. Otherwise, for the same advance coefficient, neither the thrust identity nor the torque identity is valid.

Acknowledgement:

We would like to thank Professor B. Hamoudi and Professor Z. Lakmeche, for their patient instruction, passionate support, and constructive criticisms of this study effort.

References

Abdel-Maksoud, M., Menter, F., and Wuttke, H. (1998). Viscous flow simulations for conventional and high-skew marine propellers. Ship Technology Research 45, Schiffstechnik, 45(2), 64-71.

Abbott, I. H., and Von Doenhoff, A. E. (1959). Theory of wing sections: including a summary of airfoil data. Dover Publications, Inc. New York. ISBN : 486-60586-8.

Bertram, V., (2000). Practical ship hydrodynamics. Butterworth-Heinemann, Elsevier. ISBN 0 7506 4851 1.

Blevins, R.D., (1984). Applied fluid dynamics handbook. Van Nostrand Reinhold Co., New York, N.Y.

Belhenniche, S.E., Aounallah, M., Imine, O., Celik, F., (2012). Application of CFD in Analysis of Steady and Unsteady Turbulent Flow past a Marine Propeller, in: Proceeding of THMT-12. Proceedings of the Seventh International Symposium On Turbulence, Heat and Mass Transfer Palermo, Italy, 24-27, Begellhouse, https://doi.org/10.1615/ICHMT.2012.ProcSevIntSympTurbHeatTransfPal.500

Boussinesq, J. (1877). Essai sur la théorie des eaux courantes. Paris. Imprimerie. nationale. MDCCCLXXVII.

Baker, C., (2004). Estimating Drag Forces on Submarine Hulls. Doctoral dissertation, University of New Brunswick Department of Mechanical Engineering.

Berger, S., Druckenbrod, M., Greve, M., Abdel-Maksoud, M., Greitsch, L., (2011). An efficient method for the investigation of propeller hull interaction. 14th Numerical Towing Tank Symposium–NUTTS.

Cable, M., (2009). An evaluation of turbulence models for the numerical study of forced and natural convective flow in Atria, Doctoral dissertation, Queen's University.

Cai, W., Li, Y., Liu, C., (2019). Comparative Study of Scale-resolving Simulations for Marine-Propeller Unsteady Flows. International Communications in Heat and Mass Transfer 100, 1–11. https://doi.org/10.1016/j.icheatmasstransfer.2018.10.009.

Carrica, P. M., Castro, A. M., Stern, F., (2010). Self-propulsion computations using a speed controller and a discretized propeller with dynamic overset grids. J Mar Sci Technol 15, 316–330. https://doi.org/10.1007/s00773-010-0098-6

Carrica, P. M., Huang, J., Noack, R., Kaushik, D., Smith, B., Stern, F., (2010). Large-scale DES computations of the forward speed diffraction and pitch and heave problems for a surface combatant. Computers and Fluids 39, 1095–1111. https://doi.org/10.1016/j.compfluid.2010.02.002.

Carrica, P. M., Kim, Y., Martin, J. E. (2019). Near surface self-propulsion of a generic submarine in calm water and waves. Journal of Ocean Engineering 183, 87–105

Carlton, J.S., (2019). Marine propellers and propulsion. Butterworth-Heinemann, Elsevier, ISBN: 978-0-08-100366-4.

Chase, N., Carrica, P.M., (2013). Submarine propeller computations and application to self-propulsion of DARPA Suboff. Ocean Engineering 60, 68–80. https://doi.org/10.1016/j.oceaneng.2012.12.029.

Chase, N., Michael, T., Carrica, P.M., (2013). Overset simulation of a submarine and propeller in towed, self-propelled and manoeuvring conditions. International Shipbuilding Progress 171–205.

Degiuli, N., Farkas, A., Martić, I., Zeman, I., Ruggiero, V., and Vasiljević, V., (2021). Numerical and experimental assessment of the total resistance of a yacht. Brodogradnja: Teorija I praksa brodogradnje I pomorske tehnike, 72(3), 61-80. http://dx.doi.org/10.21278/brod72305.

Di Felice, F., Felli, M., Liefvendahl, M., and Svennberg, U. (2009). Numerical and experimental analysis of the wake behaviour of a generic submarine propeller. First International Symposium on Marine Propulsors smp'09, Trondheim, Norway, 1(8), 158.

Dogrul, A., (2022). Numerical prediction of scale effects on the propulsion performance of Joubert BB2 submarine. Brodogradnja: Teorija i praksa brodogradnje i pomorske tehnike, 73(2), 17-42. http://dx.doi.org/10.21278/brod73202

Dogrul, A., Sezen, S., Delen, C., Bal, S., (2017). Self-Propulsion Simulation of Darpa Suboff. Developments in Maritime Transportation and Harvesting of Sea Resources. CRC Press, PRT. ISBN 9780815379935

Dong, K., Wang, X., Zhang, D., Liu, L., Feng, D. (2022). CFD research on the hydrodynamics performance of submarine sailing near the free surface with long-crested waves. Journal of Marine Science and Engineering (10) 1.

ITTC (2011)– Recommended Procedures and Guidelines.

ITTC, I, (2011). ITTC – Recommended Procedures and Guidelines 13.

Kerwin, J. E., Kinnas, S. A., Lee, J. T., and Shih, W.Z., (1987). A surface panel method for the hydrodynamic analysis of ducted propellers. Massachusetts Inst of Tech Cambridge Dept of Ocean Engineering.

Kalkan, O.O., (2014). Implementation of k-epsilon turbulence models in a two-dimensional parallel Navier-stokes solver on hybrid grids. Master Science thesis. Middle East Technical University.

Kinaci, O.K., Gokce, M.K., Alkan, A.D., Kukner, A., (2018). On self-propulsion assessment of marine vehicles. Brodogradnja: Teorija i praksa brodogradnje i pomorske tehnike, 69(4), 29-51. http://dx.doi.org/10.21278/brod69403

Launder, B.E., Sharma, B.I., (1974). Application of the energy-dissipation model of turbulence to the calculation of flow near a spinning disc. Letters in Heat and Mass Transfer 1, 131–137. https://doi.org/10.1016/0094-4548(74)90150-7.

Launder, B.E., Spalding, D.B., (1974). The numerical computation of turbulent flows. Computer Methods in Applied Mechanics and Engineering 3, 269–289.

https://doi.org/10.1016/0045-7825(74)90029-2

Lee, S.W., Hwang, Y.S., Ryu, M.C., Kim, I.H., Sin, M.S., (2003). A development of 3000-ton class submarine and the study on its hydrodynamic performances. Presented at the Thirteenth International Offshore and Polar Engineering Conference, International Society of Offshore and Polar Engineers.

Molland, A.F., Turnock, S.R., Hudson, D.A., (2017). Ship Resistance and Propulsion: Practical Estimation of Ship Propulsive Power, 2nd ed. Cambridge University Press, Cambridge. ISBN 978-1-107-14206-0 https://doi.org/10.1017/9781316494196

Mizzi, K., Demirel, Y.K., Banks, C., Turan, O., Kaklis, P., Atlar, M., (2017). Design optimisation of Propeller Boss Cap Fins for enhanced propeller performance. Applied Ocean Research 62, 210–222. https://doi.org/10.1016/j.apor.2016.12.006

Nouri, N.M., Mohammadi, S., Zarezadeh, M., (2018). Optimization of a marine contra-rotating propeller set. Ocean Engineering 167, 397–404. https://doi.org/10.1016/j.oceaneng.2018.05.067Xhaferaj, B., 2022. Investigation on some conventional hulls forms of the predictive accuracy of a parametric software for preliminary predictions of resistance and power. Brodogradnja: Teorija i praksa brodogradnje i pomorske tehnike, 73(1), 1-22. http://dx.doi.org/10.21278/brod73101

Nouri, N. M., Mohammadi, S., (2018). Numerical investigation of the effects of camber ratio on the hydrodynamic performance of a marine propeller. Ocean Engineering 148, 632–636. https://doi.org/10.1016/j.oceaneng.2017.06.026

Nouri, N. M., Mohammadi, S., (2016). A multi-objective approach for determining the number of blades on a naca marine propeller. Brodogradnja: Teorija i praksa, brodogradnje i pomorske tehnike 67, 15–32. https://doi.org/10.21278/brod67202

Rijpkema, D., Starke, B., Bosschers, J., (2013). Numerical simulation of propeller-hull interaction and determination of the effective wake field using a hybrid RANS-BEM approach. Third International Symposium on Marine Propulsors, 421–429.

Riegels, F. W., (1961). Aerofoil Sections. Translated from the German by D. G. Randall. London Butterworths, 281 pp.

Stern, F., Wilson, R.V., Coleman, H.W., Paterson, E.G., (1999). Verification and validation of CFD simulations. Technical Report IIHR, Report no. 407. Iowa Institute of Hydraulic Research.

Sezen, S., Dogrul, A., Delen, C., Bal, S., (2018). Investigation of self-propulsion of DARPA Suboff by RANS method. Ocean Engineering 150, 258–271. https://doi.org/10.1016/j.oceaneng.2017.12.051

Xhaferaj, B., 2022. Investigation on some conventional hulls' forms of the predictive accuracy of a parametric software for preliminary predictions of resistance and power. Brodogradnja: Teorija i praksa brodogradnje i pomorske tehnike, 73(1), 1-22. http://dx.doi.org/10.21278/brod73101

Zhang, N., Zhang, S., (2014). Numerical simulation of hull/propeller interaction of submarine in submergence and near surface conditions. Journal of Hydrodynamics, Ser. B 26, 50–56. https://doi.org/10.1016/S1001-6058(14)60006-8

Zhang, D., Dong, K., Wang, X., Feng Da. (2022), Hydrodynamic interaction study during surface ship overtaking submarine. Ocean Engineering 265 (2022) 112602. https://doi.org/10.1016/j.oceaneng.2022.112602.

Zhang, D., Dong, K., Wang, X., Feng Da, Liu, L., Dakui Feng (2022). CFD research on the hydrodynamics performance of submarine sailing near the free surface with long-crested waves. Journal of Marine Science and Engineering (10) 1.https://doi.org/10.3390/jmse.2022.10010090

25th ITTC Resistance Committee (2008). Uncertainty Analysis in CFD verification and validation methodology and procedures. ITTC – Recommended Procedures and Guidelines, 7.5-03 -01-01 12.